IIETA International Information and Engineering Technology Association
Advancing the World of Information and Engineering

Journal Européen des Systèmes Automatisés
Vol. 59, No. 4, April, 2026, pp. 1099-1109
Journal homepage: http://iieta.org/journals/jesa

Probabilistic Fatigue Life Assessment of a Heavy Truck Front Axle Beam under Various Operating Conditions Using a Combined FE-MBD Approach

Tuan Dat Vu[1], Xuan Ngoc Nguyen[2*], Van Nhu Tran[1]

[1] Department of Automotive Engineering, Faculty of Mechanical Engineering, University of Transport and Communications, Ha Noi 100000, Vietnam
[2] Faculty of Automotive Engineering Technology, Industrial University of Ho Chi Minh City, Ho Chi Minh City 700000, Vietnam

Corresponding Author Email: nguyenxuanngoc@iuh.edu.vn

https://doi.org/10.18280/jesa.590420

Received: 19 February 2026
Revised: 14 April 2026
Accepted: 23 April 2026
Available online: 30 April 2026

Keywords:
fatigue life, front axle beam, finite element analysis, multibody dynamics simulation, random road roughness, survival probability, service life

ABSTRACT

The front axle beam (FAB) of a heavy truck is the primary load-bearing structure. It is frequently subjected to dynamic loads from an uneven road surface, which can lead to fatigue failure. Therefore, assessing the fatigue strength of the FAB is always a top priority in design. In this paper, a combined method of finite element (FE) analysis and multibody dynamic (MBD) simulation is applied to determine fatigue stress under excitation from random road roughness. Fatigue analysis models of AISI 1045 and AISI 4135 materials are developed based on the S-N curve approach, incorporating the survival probability. Fatigue life at higher survival probability levels is extrapolated from the mean life corresponding to a survival probability of P(50%). The fatigue life of the FAB constructed from the two typical materials is calculated, considering the effects of various road classes, vehicle speeds, and survival probability levels. The results indicate that the fatigue life of critical positions meets durability requirements under the combined operational mode, surpassing the vehicle's expected service life of 20 years. The model and analytical methods, along with the results of this study, provide important information for designing and evaluating the fatigue strength of FAB.

1. INTRODUCTION

The front axle assembly of trucks performs several important functions. It assists steering control, distributes loads evenly across the wheels, and receives and transmits interaction forces between the wheels and the chassis frame. Typically, it supports about 30–40% of the vehicle's total weight. There are two main types of front axles for trucks: the drive axle and the dead axle. The dead axle is more commonly used for trucks, with main components including a front axle beam (FAB) and steering knuckles, which are connected to each other via kingpins, as shown in Figure 1.

During vehicle operation, FAB is subjected to various types of loads, encompassing both static and dynamic loads. These are vertical forces from sprung masses, longitudinal inertial forces when braking and accelerating, lateral forces when turning, dynamic loads from road roughness, and so on. These loads create complex stress states in the structure, especially cyclic stresses, which can lead to fatigue failure. Fatigue failure often leads to serious consequences and seems to occur without any prior warning. When a structure is subjected to a single load, the static strength is evaluated based on the material's yield strength or ultimate strength. But when it is subjected to cyclic load, fatigue failure can occur at stress levels significantly lower than the material's static strength [1]. Therefore, ensuring the fatigue strength of the FAB throughout the vehicle's service life is always a top priority when designing the product.

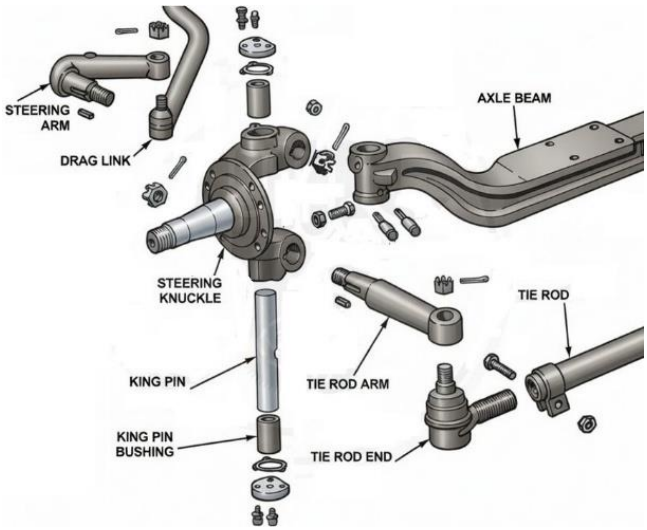

Figure 1. Typical configuration of the front axle

As computer technology has advanced, the finite element (FE) method [2] is now employed in many fields, like structural mechanics, fluid mechanics, electromagnetic fields,

etc., to design and analyze complex structures and environments [3, 4]. The FE method is an effective tool for stress analysis and identifying critical positions where failures may occur [5]. Surveys of the structural design and analysis of a truck's FAB show that all involve the application of the FE method.

Dey et al. [6] studied the load capacity for the FAB of a light commercial vehicle. The stress, strain, and deformation of the structure were determined under vertical, braking, and cornering load conditions. Datti et al. [7] calculated the vertical load on the front axle of the truck under various driving conditions, including uphill, downhill, and level roads. The stress and strain of the FAB were obtained from static analysis. Sivaraman et al. [8] studied how different shapes of alternative components affected stress and strain distribution in the FAB of a heavy commercial vehicle. The best shape of the FAB was selected from static analysis under specific load situations and driving torque needs. Avikal et al. [9] conducted fatigue life analysis for the FAB with 5 different materials: 50 steel, AISI 1045, AISI 4130, AISI 4140, and AISI 4150. The effects of states without and with cracks on fatigue life were taken into account. Verma and Pant [10] implemented a stress analysis for FAB with materials from AISI 1045 and AISI 1053. The fatigue life was predicted with different crack angles and directions. To make the FAB of a commercial vehicle lighter while ensuring mechanical strength, Ruban and Sivaganesan [11] conducted optimal analysis for three concept designs of the FAB with static load cases, including vertical, braking, and cornering loads. Fatigue analysis was carried out with sinusoidal vertical loads and combined vertical and braking loads. With 50 steel as the fabrication material, Zhang et al. [12] conducted stress and fatigue analysis for the FAB of a heavy-duty truck under sinusoidal vertical loading. The structure was improved to reduce stress concentration and increase fatigue life. Fatigue simulations with multi-working conditions and the effect of a crack's length and depth on its fatigue life were carried out. To determine the cause of premature failure at the kingpin hole and propose a structural improvement plan, Guo et al. [13] performed static strength and fatigue failure analysis for the FAB of a mining truck. Symmetrical dynamic loads were applied to the FE model for fatigue analysis. The failure fracture at the kingpin hole was studied by both simulation and experiment methods.

The aforementioned studies have focused on static strength and fatigue life analysis with typical load cases acting on the FAB under various operating conditions. Fatigue life analysis with different materials has also been conducted, enabling more effective material selection. However, the fatigue loads applied to the FAB are confined to static loads [9, 10] or sinusoidal dynamic loads [11-13]; they do not account for dynamic loads induced by random road roughness, which act continuously throughout the vehicle's operation. On the other hand, these studies use standard parameters for material fatigue curves with a default survival probability of 50%. For primary load-bearing structures such as FAB, it needs to be considered at higher survival probability levels to enhance safety.

As is known, while experimental methods are highly accurate for collecting fatigue load data, their high cost and long implementation time are disadvantages. In limited experimental conditions, combining software packages for structural simulation and analysis partially overcomes these disadvantages. This method offers several advantages, including the ability to generate multiple simulation scenarios with many influencing factors considered, reduced experimental costs, and so on. Among them, the combined FE analysis and multibody dynamics (MBD) simulation method has become the preferred approach for stress and fatigue life analysis of the structures on transport vehicles [14-17].

The research objective of this paper is to assess the fatigue life for the FAB of a heavy truck with a payload of 8.5 tons, taking into account different material types, operating conditions, and survival probability levels. First, the FE model of the front axle assembly is constructed using ANSYS software. Next, the MBD model of the entire vehicle is built using ADAMS/View software, with the object of the front axle assembly taken from the modal neutral file of the FE model. In the MBD model, road roughness as the excitation source causing fatigue loads is simulated based on the ISO 8608:2016 standard [18], considering operating conditions including various road classes and vehicle speeds. The dynamic loads obtained from the MBD simulations are used to perform a quasi-static analysis that finds out the structural stress-time histories. In the next step, the fatigue analysis models of AISI 1045 and AISI 4135 materials in the crack initiation period are developed based on the S-N fatigue curve approach using ANSYS nCode DesignLife software, which considers the survival probability, also known as the $P_{(\%)}$-S-N curve [19]. The $P_{(50\%)}$-S-N curves for these materials are established from fatigue experimental data of equivalent materials [20]. The fatigue life of critical positions at higher survival probability levels, such as $P_{(90\%)}$, $P_{(95\%)}$, and $P_{(99\%)}$, is estimated by extrapolating from the mean life of $P_{(50\%)}$. Finally, the fatigue life of the FAB made from the two typical materials is calculated, taking into account the effects of different road classes, vehicle speeds, and survival probability levels. The fatigue life in cycles is converted to operating time in years to assess the durability of the FAB against the vehicle's service life.

2. FINITE ELEMENT MODELING

2.1 Geometric model construction

ANSYS software is employed to construct the 3D model of the front axle assembly of a heavy truck, which includes the FAB, steering knuckles, and kingpins, as illustrated in Figure 2. In this model, the steering knuckles and kingpins only serve as components that receive and transmit force between the FAB and the wheel and are not objects for fatigue life analysis. The specifications of the FAB are given in Table 1.

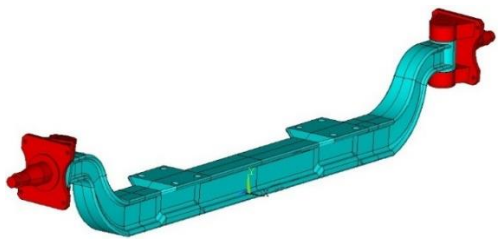

Figure 2. 3D model of the front axle assembly

2.2 Material selection

To withstand severe operating conditions, the materials chosen to make the FAB must possess outstanding mechanical properties, such as strong ultimate strength and high fatigue

strength. Reviewing the literature provided crucial data for material selection in the fatigue analysis of FAB [9, 10, 12]. Commonly chosen materials include quality carbon structural steels (AISI 10xx) and high-strength structural alloy steels (AISI 41xx). Furthermore, forging is the most common way to form the FAB, and it can be heat treated to improve durability, toughness, and corrosion resistance. Within the scope of this paper, two materials are selected: AISI 1045 (equivalent to GB 45 or JIS S45C) and AISI 4135 (equivalent to GB 35CrMo or JIS SCM435), with their basic properties given in Table 2.

Table 1. Front axle beam (FAB) specifications

Parameters (units)	Value
FAB type	Reversed elliot "I" beam
Front suspension type	Multi-leaf springs with shock absorber
Distance between the kingpin hole centers (above) (mm)	1,800
Diameter of kingpin holes (mm)	40
Caster angle (degree)	1°45'
Kingpin inclination (degree)	7°30'

Table 2. Material properties

Parameters (units)	AISI 1045	AISI 4135
Density (kg/m^3)	7,850	7,850
Elastic modulus (MPa)	2.1E+05	2.10E+5
Poisson ratio	0.29	0.29
Ultimate strength, σ_u (MPa)	620	920
Yield strength, σ_y (MPa)	370	750
Heat treatment	Normalizing at 850 ℃ (holding for 50 minutes)	Oil quenching at 850 ℃, tempering at 550 ℃ followed by oil cooling

2.3 Mesh generation

Meshing is used to model and divide the structure into a finite number of elements and nodes. This procedure is a crucial task when constructing the FE model because the size, shape, and number of elements greatly affect the accuracy of the analysis results.

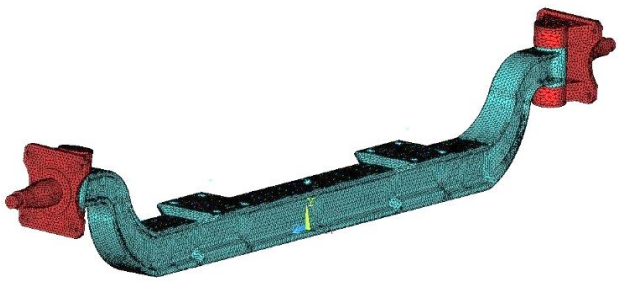

Figure 3. Finite element (FE) model of the front axle assembly

Based on the geometry and size of the 3D model, the meshing process is carried out with a tetrahedral shape chosen for the solid element and an edge size not exceeding 8.0 mm. The FE model of the front axle assembly consists of 312,866 solid elements and 65,466 nodes, as shown in Figure 3.

The contact pairs include the contact surfaces between the kingpins and the kingpin holes of the axle beam, as well as the contact surface between the steering knuckles and the axle beam (upper and lower support surfaces). These contact pairs are simulated using Targe170 and Conta174 elements with a friction coefficient of 0.1. Six interface nodes are created to act as connection points to other objects in the vehicle's MBD model. These nodes are linked to other nodes in the front axle assembly using rigid regions, including connection points between wheels and steering knuckles (two interface nodes linked to the bearing support surfaces of the wheel spindle), front leaf spring assemblies and an axle beam (two interface nodes linked to leaf spring seats), and front shock absorbers and an axle beam (two interface nodes linked to the mounting surfaces of shock absorber brackets). Now, the FE model of FAB has 315,441 elements and 65,473 nodes.

2.4 Modal neutral file generation

The "ANSYS-ADAMS Interface" feature is implemented to create a modal neutral file (*.mnf). During execution, interface nodes are selected as connection points in the MBD model. This file contains the parameters of the FE model, such as mass, center of mass position, moment of inertia, etc.

3. VEHICLE MULTIBODY DYNAMICS SIMULATION

3.1 Vehicle multibody dynamics modeling

The MBD model of the entire vehicle is constructed using ADAMS/View software. Import the modal neutral file to create the front axle assembly's object, which is considered a rigid body. The other bodies are connected to each other and to the front axle assembly using appropriate joints and elements through the interface nodes. Figure 4 shows the vehicle's MBD model that has 7 degrees of freedom (DOFs). The front and rear axles each have two DOFs: the roll angle

and the vertical displacement. The sprung mass (including the chassis, cabin, cargo body, payload, etc.) has three DOFs: the roll angle, the pitch angle, and the vertical displacement. Table 3 provides the basic parameters of this model [21, 22].

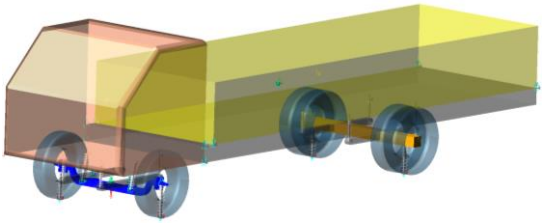

Figure 4. Multibody dynamic (MBD) model of the entire vehicle

3.2 Road roughness simulation

In the MBD model, the uneven road surface is considered the only source of excitation causing vehicle vibrations. The road roughness continuously impacts the wheels, causing the vehicle to oscillate in the vertical, roll, and pitch angle directions, which are the main causes of fatigue loads on the FAB. To simulate road roughness, the studies have assumed that the road surface profile is a stable random process following a Gaussian distribution and utilized the vertical displacement power spectral density (PSD) as its representative [23-29]. The PSD of the road surface profile can be described in Eq. (1) according to ISO 8608:2016 [18]. On that basis, this standard has given eight road classes, from class A to class H, corresponding to the lower limit, upper limit, and geometric mean value of the PSD.

$$G_q(n) = G_q(n_0)\left(\frac{n}{n_0}\right)^{-w} \quad (1)$$

where, n and n_0 refer to the spatial frequency and the referenced spatial frequency, respectively, with n_0 set at 0.1 (m^{-1}); $G_q(n_0)$ indicates the PSD of road surface roughness (m^3) when n equals n_0; w represents the frequency index, which is typically $w = 2$. The value of n falls within the effective spatial frequency range (n_1, n_2), which must include the main natural frequency of the vehicle at an average speed.

Table 3. Multibody dynamic (MBD) model parameters

Parameters (units)	Value	Parameters (units)	Value
Overall Dimension (L × W × H) (mm)	9,410 × 2,425 × 2,630	Gross vehicle mass (kg)	15,100
Wheelbase (mm)	5,530	Front axle load (kg)	5,100
Front track width (single tires) (mm)	1,920	Rear axle load (kg)	10,000
Rear track width (dual tires) (mm)	1,820	Tire size	10.00-R20
Front unsprung mass (including leaf spings) (kg)	665	Damping coefficient of each front shock absorber (N.s/mm)	8
Rear unsprung mass (including main and helper leaf spings) (kg)	1,320	Damping coefficient of a single tire (N.s/mm)	2.0
Mass of the cabin with 3 people (kg)	645	Stiffness of each front leaf spring (N/mm)	350
Mass of the cargo body with full load (kg)	10,225	Stiffness of each rear leaf spring (N/mm)	700
Other sprung mass (kg)	2,245	Stiffness of a single tire (N/mm)	850

Based on ISO 8608:2016 [18], there are many methods for simulating excitation signals from road surface profiles in the frequency and time domains. Among them, the Inverse Fast Fourier Transform (IFFT) method is often utilized when studying vehicle dynamics or road roughness simulation [23, 24, 26, 28]. This method not only generates a PSD that is more consistent with the specified one but also takes into account vehicle speed. The basic contents of the IFFT method are first converted from spatial frequency to time frequency. Next, road roughness data, according to the PSD, is discretized by the Fourier transform and added with certain rules. Finally, the IFFT method is employed to convert the existing data into road roughness in the time domain.

For truck vehicles, the operating road conditions are relatively diverse, including excellent-quality highways or good-quality interprovincial roads (which can be rated to road class A or B), normal urban or interprovincial roads (road class C), and poor-quality suburban roads (road class D). Following the recommendations for maximum speeds applied when analyzing vehicle vibration according to road classes [29], this paper selects operating conditions to simulate road surface roughness: v = 100 km/h (27.78 m/s) for road class B (denoted as the operating condition of B-V100); v = 60 km/h (16.67 m/s) for road class C (operating condition of C-V60); and v = 20 km/h (5.56 m/s) for road class D (operating condition of D-V20). Figure 5 presents a partial excerpt of the simulation results for road roughness over a 20-second period under three operating conditions.

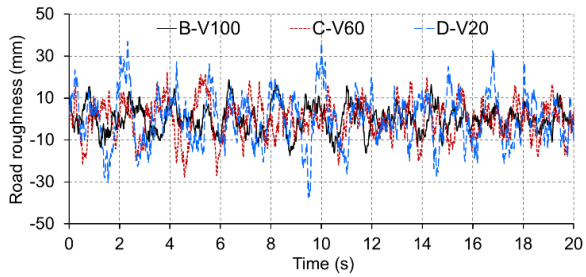

Figure 5. Simulation results of road roughness under various operating conditions

3.3 Dynamic load extraction from simulation results

Using road roughness corresponding to operating conditions B-V100, C-V60, and D-V20 as the vibration excitation source, dynamic simulations are performed for the entire vehicle's MBD model. The simulation process is

executed in 10 seconds with a sampling time step of 0.01 seconds. After the simulation, the "Export FEA Loads" feature in ADAMS/View is implemented to export the load file (*.lod). There are 1,000 load steps in each load file that act on the six interface nodes of the front axle assembly. Each load step contains data on force and torque, as well as inertial loads like angular velocity (omega), angular acceleration (domega), and acceleration along the X, Y, and Z axes.

4. STRUCTURAL STRESS ANALYSIS

A quasi-static analysis [5] is carried out for the FE model of the front axle assembly with loads applied corresponding to the operating conditions of B-V100, C-V60, and D-V20. The nodal stress-time histories are one of the crucial analytical outcomes utilized to determine critical positions and calculate fatigue life. Figure 6 displays the Von Mises stress distribution of the FAB at the 10th load step of the D-V20 operating condition.

Stress concentration zones can be seen at the following positions: (a) at the lower edge of the kingpin hole (at node 36948), (b) on the lower surface of the gooseneck (at node 10306), and (c) at the contact edge corner between the leaf spring seat and the axle beam (at node 62319). This result can be explained by the fact that position (a), in addition to directly bearing dynamic loads due to road surface roughness through the steering knuckle, also experiences friction with the kingpin. Due to the changing cross-section and the presence of a bending point, position (b) generates higher stress than neighboring areas. Through the front suspension system, position (c) is directly affected by the sprung mass and the damping force exerted by the shock absorber. Considering each load step corresponding to the same operating condition, the maximum stress is ranked in order: position (a) is the higher, followed by position (b) and position (c).

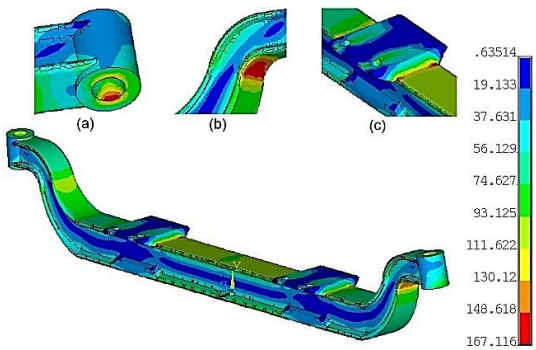

Figure 6. Von Mises stress distribution (MPa) of the front axle beam (FAB) at the 10th load step of the D-V20 operating condition

Figure 7 presents the Von Mises stress-time histories of the critical nodes under various operating conditions. The maximum stress value of 179.52 MPa appears at node 36948, corresponding to operating condition D-V20 at the 356th load step. The maximum stress values at these critical points are all lower than the yield strength of the AISI 1045 and AISI 4135 materials, which are 370 MPa and 750 MPa, respectively. This result indicates that the structure operates in the elastic region of the material.

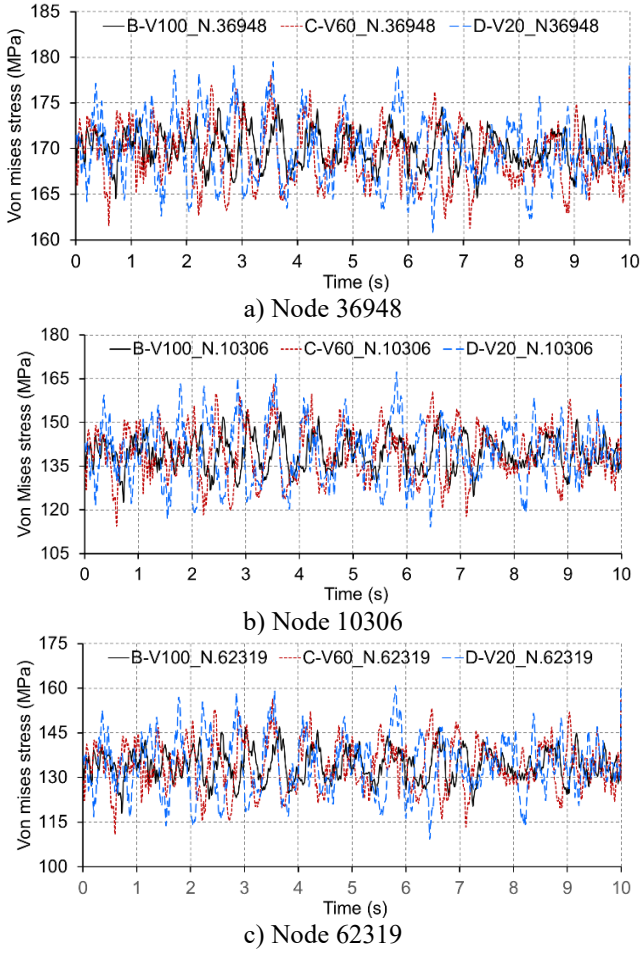

Figure 7. Stress-time histories of the critical nodes under various operating conditions

5. DEVELOPMENT OF THE FATIGUE ANALYSIS MODEL

5.1 The $P_{(50\%)}$-S-N curve establishment

The stress analysis findings demonstrate that all nodal stress values are lower than the material's yield strength. Consequently, the fatigue analysis model is applied in the crack initiation period and is developed based on the S-N fatigue curve approach, commonly referred to as the stress-life method [19]. Figure 8 illustrates a typical S-N curve of the material, representing the relationship between the amplitude or range of cyclic stress (S) and the number of cycles (N) until a fatigue crack occurs, which is often plotted on a logarithmic coordinate system. S_{RI1} and S_e denote the stress amplitudes associated with N = 1.0 and N_{C1} = 1.0E+5 to 1.0E+7 cycles, respectively. N_{C1} is considered the transitional point of life, while S_e represents the fatigue limit, and b_1 and b_2 represent the gradients of the line segments.

The standard S-N curve is often built by experimental data with different constant stress amplitude levels, each with a mean stress of S_m = 0 and a default survival probability of $P_{(50\%)}$. The collection of fatigue curves, taking into account various survival probability levels, is referred to as the family of $P_{(\%)}$-S-N curves, which can be represented by Eq. (2) [19], where a_P and b_P denote the experimental regression coefficients.

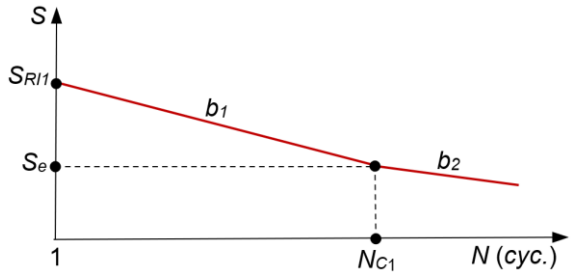

Figure 8. Typical *S-N* curve

$$\lg(N_{P(\%)}) = a_P + b_P \lg(S) \tag{2}$$

The $P_{(50\%)}$-*S-N* curves of AISI 1045 and AISI 4135 materials are established in ANSYS-nCode DesignLife software using experimental data for notched specimens of two equivalent materials, GB 45 and GB 35CrMo [20], as given in Table 4. The linear regression method is applied to estimate the coefficients a_P and b_P. With the choice of N_{C1} = 1.0E + 7 cycles, S_{RI1} and S_e values are calculated by Eq. (2), and b_1 and b_2 are derived by Eq. (3) [30]. The $P_{(50\%)}$-*S-N* curves of AISI 1045 and AISI 4135 materials are shown in Figure 9.

$$b_1 = \frac{(\lg S_e - \lg S_{RI1})}{(\lg N_{C1} - 1)};\ b_2 = \frac{b_1}{(2 + b_1)} \tag{3}$$

$$\lg(N_{P(\%)}) = \lg(N_{P(50\%)}) + SD_{P(\%)}SE \tag{4}$$

Table 4. Fatigue experimental data and $P_{(50\%)}$-S-N curve parameters of the equivalent materials

	GB 45 (AISI 1045)		GB 35CrMo (AISI 4135)	
Fatigue experimental data	*S* (MPa)	$N_{P(50\%)}$ (×10³ cyc.)	*S* (MPa)	$N_{P(50\%)}$ (×10³ cyc.)
	309	26.9	353	89.2
	270	69.9	314	169.9
	231	211.4	284	290.7
	201	553.1	265	429.4
	181	1139.0	-	-
Calculated	$a_P \approx 21.8803$; $b_P \approx -7.0069$; $S_{RI1} \approx 1{,}326.37$ MPa; $S_e \approx 132.94$ MPa; $b_1 \approx -0.14271587$; $b_2 \approx -0.07684117$.		$a_P \approx 18.8725$; $b_P \approx -5.4643$; $S_{RI1} \approx 2{,}842.88$ MPa; $S_e \approx 148.84$ MPa; $b_1 \approx -0.18300458$; $b_2 \approx -0.10071824$.	

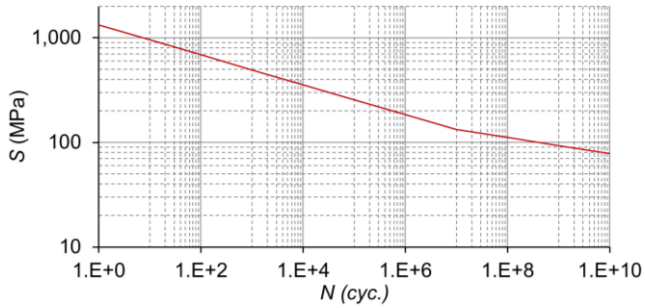

a) AISI 1045

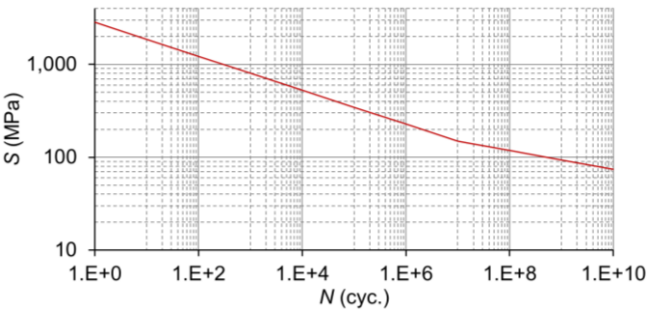

b) AISI 4135

Figure 9. $P_{(50\%)}$-*S-N* curves of the materials

In fatigue analysis, structures subjected to primary load-bearing, such as FAB, must account for higher survival probability values. Under limited experimental conditions, fatigue life with different survival probabilities is extrapolated via the mean life of $P_{(50\%)}$ using Eq. (4) [30]. The standard error (*SE*) is usually set at 0.1, whereas the standard deviation (*SD*) is derived from its correlation with $P_{(\%)}$, as illustrated in Figure 10 [30].

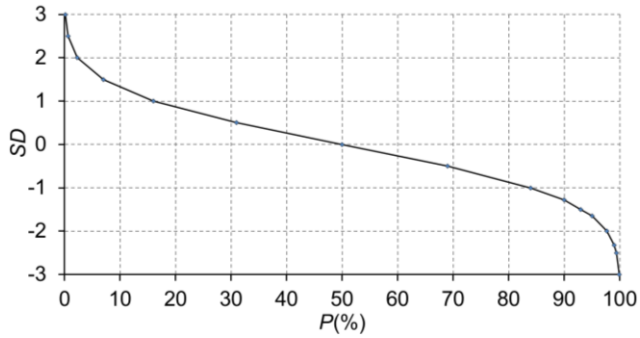

Figure 10. Correlation between standard deviation (SD) and $P_{(\%)}$

5.2 Mean stress correction method

Most structures subjected to loads in practice have cyclic fatigue stresses that are often asymmetrical with $S_m \neq 0$. This phenomenon has a significant impact on fatigue strength in the high-cycle fatigue region (N > 1.0E+4 cycles). When $S_m > 0$ (tension), it is detrimental, and when $S_m < 0$ (compression), it is beneficial for fatigue strength. Several classical correction methods have been proposed to consider the effect of mean stress on fatigue strength, such as those of Gerber, Goodman, and Soderberg [19]. The stress analysis results indicate that the Goodman correction method, described in Eq. (5) [19], is proposed as appropriate because it is linear and effective in cases of tensile mean stress at the fatigue limit.

$$\frac{S}{S_e} + \frac{S_m}{\sigma_u} = 1 \tag{5}$$

5.3 Fatigue damage evaluation

Random road roughness additionally affects the nodal stress-time histories in the FAB, which are characterized by variable amplitude and an asymmetric profile. In ANSYS-nCode DesignLife software, the rainflow counting method [19, 31] is employed to statistically compute the parameters of the stress cycle. The counting results will ascertain the number of stress cycles (n_i) corresponding to each stress amplitude level (S_i), from which the fatigue life (N_i) will be calculated based on the established fatigue curve. It enables the application of the Miner damage rule expressed in Eq. (6) [32] to determine fatigue damage (D_i). During the crack initiation period, a fatigue crack will appear when accumulated fatigue damage (D_Σ) attains the threshold value of 1.0.

$$D_\Sigma = \sum D_i = \sum \frac{n_i}{N_i} \tag{6}$$

6. FATIGUE LIFE PREDICTION OF THE FRONT AXLE BEAM

6.1 Fatigue life under individual operating conditions

The stress analysis result files (*.rst) are successively imported into the constructed fatigue analysis models to calculate the fatigue life of the FAB structure. Figure 11 shows the fatigue life distribution of the FAB structure for AISI 1045 and AISI 4135 under various operating conditions at a survival probability of $P_{(50\%)}$. The results indicate that the critical positions are located in the area of the kingpin hole box (at node 36948). Based on the mean life at $P_{(50\%)}$, the fatigue life at survival probability levels $P_{(90\%)}$, $P_{(95\%)}$, and $P_{(99\%)}$ are calculated using Eq. (4). The standard deviations for the probability levels are set to $SD_{(90\%)}$ = -1.2816, $SD_{(95\%)}$ = -1.6449, and $SD_{(99\%)}$ = -2.3263 [30]. Table 5 lists the calculated minimum fatigue life in cycles of the FAB's critical positions for two typical materials under various operating conditions and survival probability levels. The minimum fatigue life in cycles ($N_{\min}$) is converted into vehicle operating time in years (T_y) using an intermediate quantity representing the vehicle travel distance in kilometers (L_{td}), as described by Eqs. (7) and (8). These equations are implemented based on the following assumptions: the daily operation time of the vehicle at full load, h_d = 7 hours, does not include the stopping time for loading and unloading; the utilization coefficient, α_u = 0.7; and the number of days in a year, d_y = 365 days. The charts in Figures 12 and 13 display the vehicle travel distance and the operating time, which are derived from the minimum fatigue life value of the FAB's critical positions.

$$L_{td} = N_{\min} L_j = N_{\min} t_{sm} . v_j \tag{7}$$

$$T_y = \frac{L_{td}}{v_j h_d \alpha_u d_y} = \frac{N_{\min} t_{sm}}{h_d \alpha_u d_y} \tag{8}$$

where, L_j represents the vehicle travel distance for each operating condition within the simulation time, $L_{B\text{-}V100}$ = 0.277 km, $L_{C\text{-}V60}$ = 0.167 km, and $L_{D\text{-}V20}$ = 0.056 km; t_{sm} denotes the simulation time, t_{sm} = 0.0277 hours (10 seconds); and v_j indicates the vehicle speed, $v_{B\text{-}V100}$ = 100 km/h, $v_{C\text{-}V60}$ = 60 km/h, and $v_{D\text{-}V20}$ = 20 km/h.

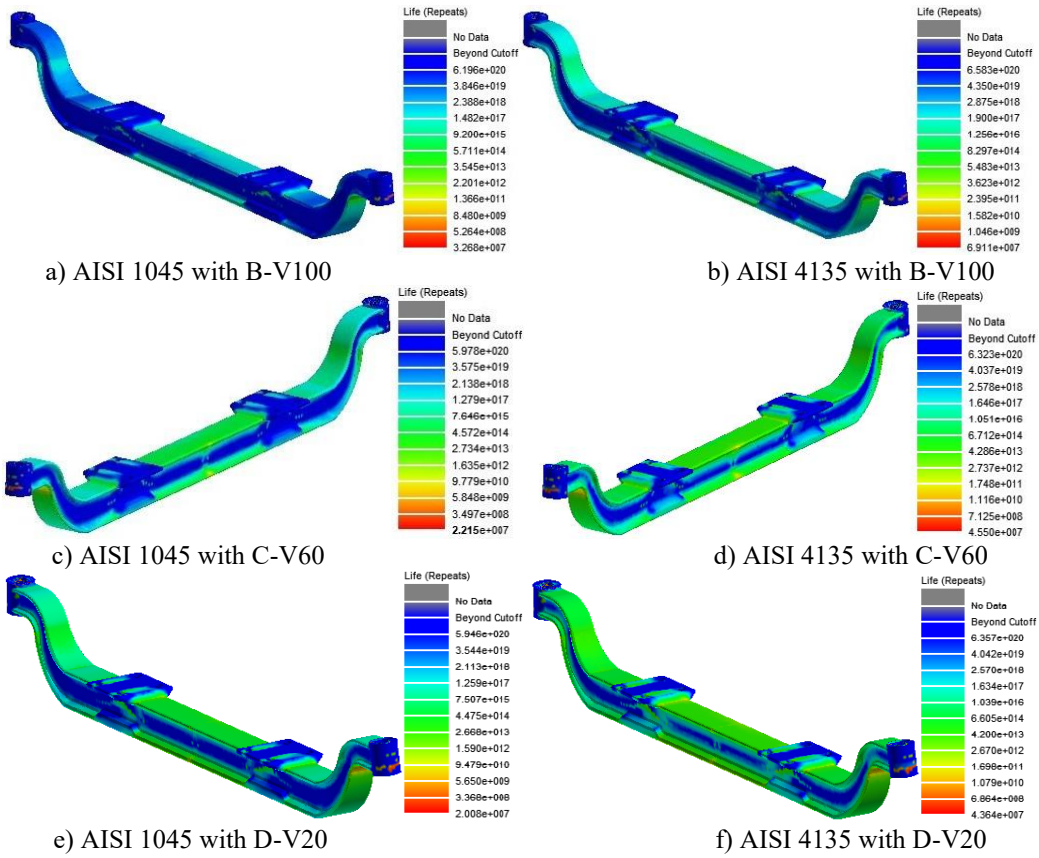

Figure 11. Fatigue life distribution (cycles) of the front axle beam (FAB) for AISI 1045 and AISI 4135 under various operating conditions at a survival probability of $P_{(50\%)}$

Table 5. Minimum fatigue life (cycles) of the front axle beam (FAB) for AISI 1045 and AISI 4135 under various operating conditions and survival probability levels

$P_{(\%)}$	AISI 1045			AISI 4135		
	B-V100	C-V60	D-V20	B-V100	C-V60	D-V20
$P_{(50\%)}$	3.27E+07	2.22E+07	2.01E+07	6.91E+07	4.55E+07	4.36E+07
$P_{(90\%)}$	2.43E+07	1.65E+07	1.49E+07	5.14E+07	3.39E+07	3.25E+07
$P_{(95\%)}$	2.24E+07	1.52E+07	1.37E+07	4.73E+07	3.12E+07	2.99E+07
$P_{(99\%)}$	1.91E+07	1.30E+07	1.18E+07	4.04E+07	2.66E+07	2.55E+07

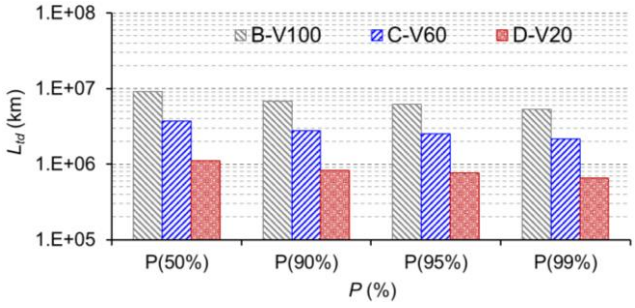

a) AISI 1045

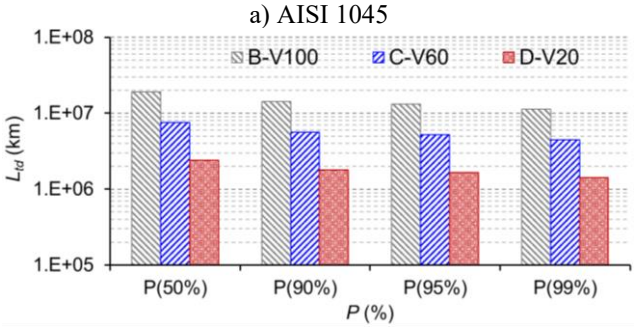

b) AISI 4135

Figure 12. Vehicle travel distance (km) corresponding to the minimum fatigue life of the FAB for AISI 1045 and AISI 4135 under various operating conditions and survival probability levels

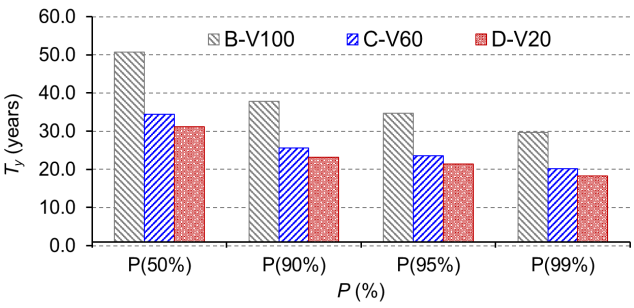

a) AISI 1045

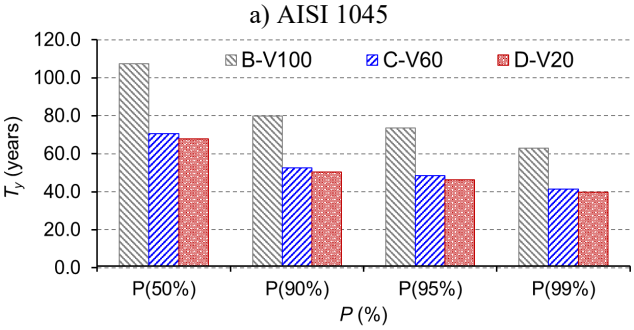

b) AISI 4135

Figure 13. Vehicle operating time (years) corresponding to the minimum fatigue life of the FAB for AISI 1045 and AISI 4135 under various operating conditions and survival probability levels

Fatigue life calculations indicate that the FAB, made of AISI 1045, which is a type of quality carbon structural steel, appears appropriate for light or medium load conditions. AISI 4135, another type of high-strength structural alloy steel, has a significantly higher fatigue life than AISI 1045, making it more suitable for heavy load conditions and requiring a longer fatigue life. However, easier processing and lower cost are advantages of AISI 1045 when choosing a material for the FAB, particularly for truck manufacturers aiming to optimize production costs while ensuring adequate performance for light or medium load conditions.

Currently, most countries and regions have no specific regulations on the service life of trucks; vehicles are still utilized as long as they meet roadworthiness tests and emission standards. Some studies indicate that the service life of trucks is at an average level of about 15 years or at a high level of about 20 years [33-35]. If 20 years is chosen as the service life of the truck, then AISI 4135 meets the durability requirements under various operating conditions and at all specified survival probability levels. Meanwhile, AISI 1045 does not seem to meet the durability requirement under operating conditions of D-V20 and at a survival probability level of $P_{(99\%)}$, with T_y = 18.25 years, indicating that it may not be suitable for long-term use in this context compared to AISI 4135.

Table 6. Characteristic values of FAB's fatigue strength for AISI 1045 and AISI 4135 under a combined operating mode

$P_{(\%)}$	AISI 1045			AISI 4135		
	N_Σ (cyc.)	L_Σ (km)	T_Σ (years)	N_Σ (cyc.)	L_Σ (km)	T_Σ (years)
$P_{(50\%)}$	7.97E+6	3.98E+06	37.1	1.68E+7	8.42E+06	78.5
$P_{(90\%)}$	5.93E+6	2.96E+06	27.6	1.25E+7	6.27E+06	58.4
$P_{(95\%)}$	5.45E+6	2.73E+06	25.4	1.15E+7	5.77E+06	53.7
$P_{(99\%)}$	4.66E+6	2.33E+06	21.7	9.86E+6	4.93E+06	45.9

Note: FAB = front axle beam

6.2 Fatigue life under a combined operating mode

The fatigue life assessment under individual operating conditions aims to evaluate the influence of each case on the fatigue life of the FAB. However, this approach seems unsuitable for actual utilization conditions when assuming the vehicle operates on only one road class with a single vehicle speed throughout its service life. Consider the combined operating mode of the vehicle on various road classes and vehicle speeds, including B-V100, C-V60, and D-V20. Each case has the same operating time, corresponding to the same simulation time. Assume that the critical position with the maximum cumulative fatigue damage in each case is at the same node. The total accumulated fatigue damage (D_Σ) is calculated using Eq. (9). The total travel distance (L_Σ) and total operating time (T_Σ) of the vehicle are calculated using Eq. (10) and Eq. (11).

$$D_{\Sigma} = \sum D_j = D_{B-V100} + D_{C-V60} + D_{D-V20} \quad (9)$$

$$L_{\Sigma} = N_{\Sigma} \sum L_j = \frac{(L_{B-V100} + L_{C-V60} + L_{D-V20})}{D_{\Sigma}} \quad (10)$$

$$T_{\Sigma} = \frac{N_{\Sigma} t_{\Sigma}}{h_d \alpha_u d_y} \quad (11)$$

where, D_{B-V100}, D_{C-V60}, and D_{D-V20} correspond to the cumulative fatigue damage of each operating case; and t_{Σ} denotes the total simulation time, $t_{\Sigma} = 3t_{sm}$; N_{Σ} is fatigue life corresponding to D_{Σ}.

Table 6 presents the calculation results for the characteristic values of the FAB's fatigue strength under a combined operating mode and at all specified survival probability levels. It can be seen that the minimum operating time of the FAB exceeds the 20-year vehicle service life for both materials.

7. CONCLUSIONS

This study was conducted to assess the fatigue life of a heavy truck's FAB. The structural fatigue stress was determined utilizing a combined method of FE analysis and MBD simulation. The fatigue analysis model in the crack initiation period was developed based on the $P_{(\%)}$-S-N fatigue curves of typical materials, AISI 1045 and AISI 4135. The $P_{(50\%)}$-S-N curves of these materials were generated from experimental fatigue data of equivalent materials. The fatigue life of the FAB was calculated, taking into account the effects of various operating conditions, such as road classes and vehicle speeds, and specified survival probability levels. The analysis results lead to the following main conclusions:

(1) AISI 1045 material appears appropriate for fabricating FAB under light and medium load conditions. Under heavier operating conditions, such as D-V20, and with a survival probability level of $P_{(99\%)}$, AISI 1045 material becomes unsuitable when considering the vehicle's service life of 20 years.

(2) AISI 4135 material has superior fatigue strength. Under various operating conditions and at all specified survival probability levels, the fatigue life of FAB is consistently longer than 20 years.

(3) Both material types satisfy the FAB fatigue life requirement of exceeding 20 years at all specified survival probability levels, assuming the vehicle operates in a combined mode.

Based on the methods and results obtained in this paper, optimizing the structure according to fatigue strength to reduce the weight of FAB is considered a direction for future investigation.

REFERENCES

[1] Schijve, J. (2009). Chapter 1: Introduction to fatigue of structures and materials. In Fatigue of Structures and Materials, 2nd Ed. Springer, Dordrecht, pp. 1-36.

[2] Zienkiewicz, O.C., Taylor, R.L., Zhu, J.Z. (2005). Chapter 1: The standard discrete system and origins of the finite element method. In The Finite Element Method: Its Basis and Fundamentals, 6th ed. Elsevier Butterworth-Heinemann Press.

[3] Ouyoussef, N., Moustabchir, H. (2023). Predicting fracture placement and analyzing fatigue life in exhaust manifold systems using finite element analysis. Journal Européen des Systèmes Automatisés, 56(3): 493-499. https://doi.org/10.18280/jesa.560317

[4] Chi, P.D., Huu, H.B., Quoc, V.D., Minh, D.B. (2025). Analytical and finite element methods for evaluative electromagnetic parameters of inset PMSM and SPMSM. Journal Européen des Systèmes Automatisés, 58(2): 337-343. https://doi.org/10.18280/jesa.580214

[5] Bishop, N., Sherratt, F. (2000). Finite Element Based Fatigue Calculations. NAFEMS Press, United Kingdom. ISBN 978-1-83979-008-9.

[6] Dey, S., Sri Rama Chandra Murthy, P.R.V.V.V., Baskar, P. (2014). Structural analysis of front axle beam of a light commercial vehicle (LCV). International Journal of Engineering Trends and Technology, 11(2): 208-213. https://doi.org/10.14445/22315381/IJETT-V11P241

[7] Datti, D.H., Nallamothu, R.B., Mitiku, G., Siraj, A., Fentaw, G. (2021). Design and analysis of front axle of truck at different driving conditions. In Recent Advances in Sustainable Technologies: Select Proceedings of ICAST 2020, Singapore: Springer Singapore, pp. 195-206. https://doi.org/10.1007/978-981-16-0976-3_18

[8] Sivaraman, P., Ilakiya, P., Prabhu, M.K., Ajayan, A., Nithyanandan, T. (2023). Optimizing front axle design for heavy commercial vehicles: A comprehensive analysis of structural and mechanical properties. SAE Technical Paper, No. 2023-01-5076. https://doi.org/10.4271/2023-01-5076

[9] Avikal, S., Bisht, A., Sharma, D., Hindwan, H., Yadav, S., Kumar, K.C.N., Thakur, P. (2020). Design and fatigue analysis of front axle beam of a heavy-duty truck using Ansys. Materials Today Proceedings, 26(2): 3211-3215. https://doi.org/10.1016/j.matpr.2020.02.901

[10] Verma, R.P., Pant, S. (2021). Fatigue life prediction of front axle of truck at different crack directions using ANSYS. In Advances in Engineering Design: Select Proceedings of FLAME 2020, Singapore: Springer Singapore, pp. 243-250. https://doi.org/10.1007/978-981-33-4684-0_25

[11] Ruban, M., Sivaganesan, S. (2016). Design analysis and optimization of front axle for commercial vehicle using CAE. ARPN Journal of Engineering and Applied Sciences, 11(13): 8511-8516.

[12] Zhang, M., Ji, X.F., Li, L.J. (2016). A research on fatigue life of front axle beam for heavy-duty truck. Advances in Engineering Software, 91: 63-68. https://doi.org/10.1016/j.advengsoft.2015.10.006

[13] Guo, X., Yan, Z., Yu, J. (2024). Failure analysis of kingpin hole on front axle of mining truck based on finite element analysis. Engineering Failure Analysis, 166: 108888. https://doi.org/10.1016/j.engfailanal.2024.108888

[14] Do, D.T., Vu, T.D., Nguyen, D.T., Do, A.T. (2021). Fatigue life evaluation of bogie frame of railway covered goods wagons using a combined FEA/MDS approach. In Proceedings of the 3rd International Conference on Sustainability in Civil Engineering. Lecture Notes in Civil Engineering, Singapore, pp. 351-357. https://doi.org/10.1007/978-981-16-0053-1_44

[15] Kashyzadeh, K.R., Souri, K., Bayat, A.G., Jabalbarez, R.S., Ahmad, M. (2022). Fatigue life analysis of

automotive cast iron knuckle under constant and variable amplitude loading conditions. Applied Mechanics, 3(2): 517-532. https://doi.org/10.3390/applmech3020030
[16] Zhou, D., Chang, J. (2022). Fatigue analysis of a light truck rear axle based on virtual iteration method. Shock and Vibration, 2022(1): 8598491. https://doi.org/10.1155/2022/8598491
[17] Zhou, S., Liu, H., Zhu, C., Yu, H., Zhou, Y., Ran, C., Guan, X. (2024). Impact Strength Analysis of Body Structure Based on a MBD-FEA Combined Method. SAE Technical Paper, No. 2024-01-2243. https://doi.org/10.4271/2024-01-2243
[18] ISO 8608:2016. (2016). Mechanical Vibration-Road Surface Profiles-Reporting of Measured Data. International Organization for Standardization Press, Geneva, Switzerland.
[19] Lee, Y.L., Taylor, D. (2005). Chapter 4: Stress-based fatigue analysis and design. In Fatigue Testing and Analysis: Theory and Practice. Elsevier Butterworth–Heinemann Press.
[20] Editorial Committee of "Mechanical Engineering Material Properties Data Handbook". (1995). Chapter 2: Carbon steel and low-alloy steel and Chapter 3: Structural alloy steel. In Mechanical Engineering Materials Properties Data Handbook. China Machinery Industry Press.
[21] Wong, J.Y. (2001). Chapter 1: Mechanics of Pneumatic Tires. In Theory of Ground Vehicles, 3rd ed. John Wiley & Sons, Inc Press.
[22] Harwood, D.W., Torbic, D.J., Richard, K.R., Glauz, W.D., Elefteriadou, L. (2003). Chapter 5: Truck characteristics related to geometric design. In Review of Truck Characteristics as Factors in Roadway Design. NCHRP Report 505. Transportation Research Board of the National Academies Press, Washington, D.C.
[23] Ren, H.B., Chen, S.Zh., Wu, Z.C. (2011). Model of excitation of random road profile in time domain for a vehicle with four wheels. In International Conference on Mechatronic Science, Electric Engineering and Computer, Jilin, China, pp. 2332-2335. https://doi.org/10.1109/MEC.2011.6025960
[24] Hu, Z.G., Zhang, Y.L., Ye, J.P., Song, S.Y., Chen, L.P. (2011). Numerical modeling and simulation of random road surface using IFFT method. Advanced Materials Research, 199: 999-1004. https://doi.org/10.4028/www.scientific.net/AMR.199-200.999
[25] Bogsjö, K., Podgórski, K., Rychlik, I. (2012). Models for road surface roughness. Vehicle System Dynamics, 50(5): 725-747. https://doi.org/10.1080/00423114.2011.637566
[26] Dharankar, C.S., Hada, M.K., Chandel, S. (2017). Numerical generation of road profile through spectral description for simulation of vehicle suspension. Journal of the Brazilian Society of Mechanical Sciences and Engineering, 39(6): 1957-1967. https://doi.org/10.1007/s40430-016-0615-6
[27] Liu, L.X., Guo, X.R., Yang, X.Y., Liu, L.J. (2024). Combined identification of vehicle parameters and road surface roughness using vehicle responses. Applied Sciences, 14(22): 10310. https://doi.org/10.3390/app142210310
[28] Sanders, T., Mavros, G., Knowles, J. (2025). Characterisation and generation of road surface roughness for improved tyre-road interaction models. Results in Engineering, 26: 105644. https://doi.org/10.1016/j.rineng.2025.105644
[29] Múčka, P. (2018). Simulated road profiles according to ISO 8608 in vibration analysis. Journal of Testing and Evaluation, 46(1): 405-418. https://doi.org/10.1520/JTE20160265
[30] HBM United Kingdom Limited. (2013). Chapter 4: Materials. In Design Life Theory Guide. United Kingdom: HBM United Kingdom Limited, http://oss.jishulink.com/caenet/forums/upload/2014/09/25/191/45541828203375.pdf.
[31] Lee, Y.L., Taylor, D. (2005). Chapter 3: Cycle counting techniques. In: Lee, Y.L., Pan, J., Hathaway, R.B., Barkey, M.E. Fatigue Testing and Analysis: Theory and Practice. Elsevier Butterworth–Heinemann Press. ISBN 978-0-7506-7719-6.
[32] Fatemi, A., Yang, L. (1998). Cumulative fatigue damage and life prediction theories: A survey of the state of the art for homogeneous materials. International Journal of Fatigue, 20(1): 9-34. https://doi.org/10.1016/S0142-1123(97)00081-9
[33] Yang, L., Hao, C.X., Chai, Y.N. (2018). Life cycle assessment of commercial delivery trucks: Diesel, plug-in electric, and battery-swap electric. Sustainability, 10(12): 4547. https://doi.org/10.3390/su10124547
[34] Meszler, D., Delgado, O., Rodríguez, F., Muncrief, R. (2018). European heavy-duty vehicles: Cost-effectiveness of fuel-efficiency technologies for long-haul tractor-trailers in the 2025–2030 timeframe. International Council on Clean Transportation: Washington, DC, USA. https://www.theicct.org/publications/cost-effectiveness-of-fuel-efficiency-tech-tractor-trailers.
[35] Boarnet, M.G., Giuliano, G., Pilgram, C., Chen, R., Shao, Q. (2024). Navigating California's transition to zero-emission drayage trucks. METRANS Transportation Consortium, University of Southern California. https://www.metrans.org/assets/research/labc-acf-report-full-report-5.pdf.

NOMENCLATURE

B-V100	operating conditions corresponding to road class B and a vehicle speed of 100 km/h
C-V60	operating conditions corresponding to road class C and a vehicle speed of 60 km/h
D-V60	operating conditions corresponding to road class D and a vehicle speed of 20 km/h
DOF	degrees of freedom
FAB	front axle beam
FE	finite element
IFFT	inverse fast Fourier transform
MBD	multibody dynamic
PSD	power spectral density
a_P and b_P	experimental regression coefficients of $P_{(\%)}$-S-N curve
b_1 and b_2	gradients of the line segments of the fatigue curve
d_y	number of days in a year, days
D_i	fatigue damage corresponding to n_i and S_i

D_Σ	accumulated fatigue damage
$G_q(n)$	PSD of road surface roughness, m^3
h_d	daily operation time of the vehicle at full load, hours
L_j	vehicle travel distance within the simulation time, km
L_{td}	vehicle travel distance corresponding to N_{min}, km
L_Σ	vehicle total travel distance corresponding to N_Σ, km
n	spatial frequency, m^{-1}
n_0	referenced spatial frequency, m^{-1}
n_1	upper limit of spatial frequency, m^{-1}
n_2	lower limit of spatial frequency, m^{-1}
n_i	number of stress cycles corresponding to each stress amplitude level (S_i)
N	fatigue life in cycles until a fatigue crack occurs, cycles
N_{C1}	transitional point of life, cycles
N_{min}	minimum fatigue life corresponding to each operating condition, cycles
N_Σ	fatigue life corresponding to D_Σ, cycles
$P_{(\%)}$-S-N	fatigue curve considering the survival probability
S	amplitude or range of cyclic stress, MPa
SD	standard deviation
SE	standard error
S_e	fatigue limit, MPa
S_m	mean stress, MPa
S_{RI1}	stress amplitudes associated with $N = 1.0$ cycle, MPa
t_{sm}	simulation time, hours
t_Σ	total simulation time, hours
T_y	vehicle operating time corresponding to N_{min}, years
T_Σ	vehicle total operating time corresponding to N_Σ, years
v	vehicle speed, km/h
w	frequency index

Greek symbols

α_u	utilization coefficient of vehicle
σ_u	ultimate strength, MPa
σ_y	yield strength, MPa